MJSAT

Malaysian Journal of Science and Advanced Technology

journal homepage: https://mjsat.com.my/

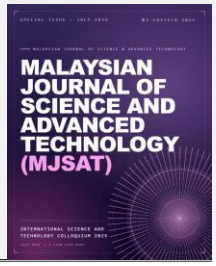

Effects of Ni^{2+} and Cr^{3+} Substitution at Mn-Site on Structural and Electrical Resistivity of Charge Ordered Divalent-Doped $Sm_{0.5}ca_{0.5}Mno_3$ Manganite

M.Z.T. Kamaruzzaman[1], R. Rozilah[*1], N.H. Abdulruhim[1], N. Ibrahim[2], and Z. Mohamed[2]

[1]*Faculty of Applied Sciences, Universiti Teknologi MARA, Perlis Branch, 02600, Arau, Perlis, Malaysia.*
[2]*Faculty of Applied Sciences, Universiti Teknologi MARA,40450, Shah Alam, Selangor, Malaysia*

KEYWORDS

Sm-Based Manganite
Ni-Substitution
Cr-Substitution
Charge Ordered
Electrical Resistivity

ARTICLE HISTORY

Received 22 November 2025
Available online 21 August 2026

ABSTRACT

Perovskite manganites ($R_{1-x}A_xMnO_3$) are widely studied for their unique magneto-transport properties, especially the metal-insulator transitions. $Sm_{0.5}Ca_{0.5}MnO_3$ is a prototypical half-doped manganite known for its strong charge-ordering (CO) behaviour and high CO temperature ($T_{CO} \approx 270$ K), which limits its practical applications due to persistent insulating characteristics. Throughout this study, the effect of partial Mn-site substitution with $Ni^{2+}$and Cr^{3+}ions in relation to the structural and electrical transport properties of $Sm_{0.5}Ca_{0.5}Mn_{1-x}A_xO_3$ (A = Ni, Cr; x = 0.07) is investigated to explore potential suppression of the CO state and the promotion of ferromagnetic metallic (FMM) behaviour. Polycrystalline of the samples were synthesized via solid-state reaction. X-ray diffraction tied with Rietveld refinement confirmed single-phase orthorhombic *pnma* structure across all samples. Substitution with Ni^{2+}resulted in an increase in unit cell volume while Cr^{3+} substitution slightly reduced it and attributed to differences in ionic radii. Both substitutions reduced the Jahn–Teller distortion; however, Cr^{3+} was more effective due to its stronger coupling with the Mn–O–Mn network and enhanced double-exchange interactions. The Ni^{2+}-substituted sample remains insulating, although its resistivity is reduced due to lattice disorder.In contrast, Cr^{3+} substitution induced a clear metallic-insulating transition at $T_{MI} = 55$ K (0 T) and 75 K (0.8 T), evidencing effective CO suppression and enhancement of double exchange driven FMM interactions. These findings demonstrate that Mn-site Cr^{3+}substitution is a promising approach for destabilizing the CO state and inducing metallic behavior in strongly CO manganites with implications for future magnetoresistive and spintronic device applications.

1. INTRODUCTION

The Perovskite manganites, expressed by the general formula $R_{1-x}A_xMnO_3$ (where R corresponding a rare earth element and A standing for an alkali or alkaline earth element), have been extensively studied for their distinctive physical and magneto-transport properties, which arise from the intricate interplay of their structural and electronic phase diagrams [1–3].Significant interest in these materials arises from the detection of colossal magnetoresistance (CMR) phenomena and the emergence of metal-insulator transition behaviours, which are crucial for the development of new electronic devices, including spintronics and magnetic sensors. Perovskite manganites display transitions between ferromagnetic and paramagnetic states, as well as between metallic and insulating phases. The ferromagnetic metallic (FMM) state mostly results out of the double exchange (DE) [4] mechanism, wherein e_g electrons transfer from Mn^{3+} to Mn^{4+} through oxygen orbitals. The Jahn–Teller (JT) [5] effect from Mn^{3+} promotes a paramagnetic insulating (PMI) state. DE alone cannot entirely explain the insulating behaviour; additional interactions also influence the system's transport and magnetic characteristics.

Previous studies on divalent half-doped manganites have shown that $Sm_{0.5}Ca_{0.5}MnO_3$ [1–3,6] exhibits a higher charge-ordering temperature ($T_{CO} \approx 270$ K) compared to $Pr_{0.5}Ca_{0.5}MnO_3$ (≈230 K) [7] and $Nd_{0.5}Ca_{0.5}MnO_3$ (≈250 K) [8]. This elevated T_{CO}, along with strong insulating behavior, limits its potential for sensor applications. The robust CO state is closely tied to structural distortion, reflected in the tolerance factor (τ); lower τ values are typically associated with stronger CO and higher T_{CO}. Despite its significance, the role of τ in stabilizing CO states remains underexplored. Substituting magnetic ions at the Mn site offers a promising route to tune lattice distortion, carrier concentration, and Mn-ion interactions, potentially weakening the CO state and enhancing the functional properties of these manganites.

*Corresponding author:
E-mail address: Rozilah Rajmi < rozilahrajmi@uitm.edu.my >.
https://doi.org/10.56532/mjsat.v6iS1.788

Many studies have shown that Mn-site substitution has a stronger effect on manganite properties than A-site substitution, as Mn ions are key to their magnetic and electronic behavior. The impact depends on the substituent's electronic configuration, ionic radius and spin state. For example, Cr^{3+} $t_{2g}^3 e_g^0$, with an electron configuration similar to Mn^{4+}, effectively suppresses the charge-ordered (CO) state and promotes a FMM phase in $Pr_{0.5}Ca_{0.5}Mn_{1-x}Cr_xO_3$ [9]. Similarly, Ni^{2+} $t_{2g}^6 e_g^2$ can induce a metal-insulator (MI) transition through superexchange interactions with Mn^{4+}, indirectly supporting DE between Mn^{3+} and Mn^{4+} ions [5,10]. However, the effects of Ni^{2+} and Cr^{3+} substitution in divalent-doped CO manganites remain largely unexplored, demanding further investigation into their role in promoting the FMM phase.

2. EXPERIMENTAL DETAILS

Polycrystalline $Sm_{0.5}Ca_{0.5}MnO_3$, $Sm_{0.5}Ca_{0.5}Mn_{0.93}Ni_{0.07}O_3$ and $Sm_{0.5}Ca_{0.5}Mn_{0.93}Cr_{0.07}O_3$ ceramics were prepared via solid-state reaction [5,6] utilizing materials in powder form with purity (>99.99%) purity of Sm_2O_3, MnO_2, $CaCO_3$, NiO and Cr_2O_3. Initially, the prepared powders were ground for two hours after being mixed in a stoichiometric ratio. This was followed by calcinations in air at 950 °C for a duration of 24 hours with periods of grinding in between [6]. To attain the target oxygen stoichiometry, the samples were first pelletized and then sintered in air at 1050 °C for 24 hours [5]. A subsequent cooling process at 1 °C/min was then employed. A PAN analytical X-ray diffractometer (model Xpert PRO MPD) alongside Cu-Kα (λ = 0.154 nm) exposure to room-temperature radiation was used to characterize the samples' structures. The data were recorded within a 2θ range of 20° to 90°. The morphology of the prepared samples was examined using a field emission scanning electron microscope (FE-SEM; NOVA NanoSEM 450, FEI, Hillsboro, Oregon, USA), while their elemental composition was determined by energy-dispersive X-ray spectroscopy (EDX). Temperature of metal-insulator transition (T_{MI}) was determined by analysing the variations under electrical resistivity through a conventional four-point probe method [6] with ohmic contacts prepared using silver paste. Measurements were carried out over a temperature range of 30–300 K under controlled temperature conditions by applying a constant current and recording the voltage drop using a nanovoltmeter, both in zero field and under an external magnetic field of 0.8 T to evaluate the magnetoresistance characteristics of the samples.

3. RESULTS AND DISCUSSION

The structural properties of our samples were studied through XRD technique at room temperature. Fig. 1 (a)-(c) illustrate the XRD pattern of $Sm_{0.5}Ca_{0.5}MnO_3$, $Sm_{0.5}Ca_{0.5}Mn_{0.93}Ni_{0.07}O_3$ and $Sm_{0.5}Ca_{0.5}Mn_{0.93}Cr_{0.07}O_3$ achieved by Rietveld refinement analysis. XRD patterns of the samples were analysed using the orthorhombic crystal structure *Pnma* (No. 62) space group where a lattice parameter $a \neq b \neq c$ and α ≠ β ≠ γ across the observed 2θ range of 10° to 90°. All samples show sharp, clear and well-defined peaks through its XRD pattern indicating high crystallinity thus proving that each sample is in single phase without secondary phases or impurities. The goodness of fit (GOF) pointer χ^2 indicates a strong correlation between the obtained and derived profiles, as evidenced by the refinement quality in Fig. 1(a)-(c).

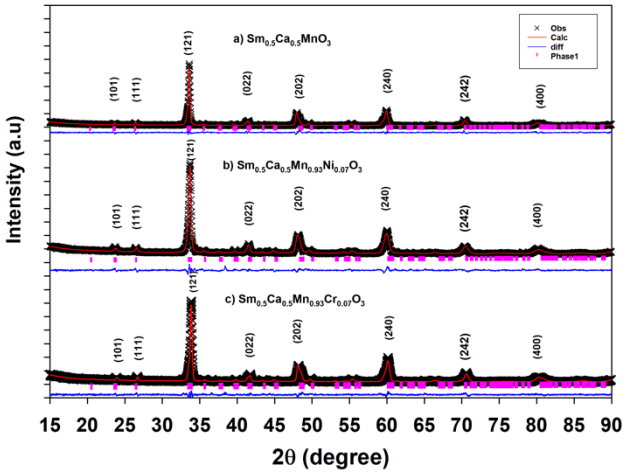

Fig. 1(a)-(c). Final Refinement of XRD patterns at room temperature for $Sm_{0.5}Ca_{0.5}MnO_3$, $Sm_{0.5}Ca_{0.5}Mn_{0.93}Ni_{0.07}O_3$ and $Sm_{0.5}Ca_{0.5}Mn_{0.93}Cr_{0.07}O_3$ samples.

Field emission scanning electron microscope (FESEM) images of $Sm_{0.5}Ca_{0.5}MnO_3$, $Sm_{0.5}Ca_{0.5}Mn_{0.93}Ni_{0.07}O_3$ and $Sm_{0.5}Ca_{0.5}Mn_{0.93}Cr_{0.07}O_3$ samples at magnification of 10,000 are shown in Fig. 2 (a)-(c). The images of $Sm_{0.5}Ca_{0.5}MnO_3$ reveals irregularly shape grains with inhomogeneous morphology and poor intergranular connectivity. Upon substituting Ni^{2+} and Cr^{3+} at x = 0.07 concentration at the $Sm_{0.5}Ca_{0.5}MnO_3$, the grains become more structured, exhibiting a more uniform shape and improved connectivity. Furthermore, an increase in grain size is observed from Cr^{3+} substitution better than pure sample and Ni^{2+} substitution concentration. The enhancement in grain size can be attributed to the reduction in grain boundaries.

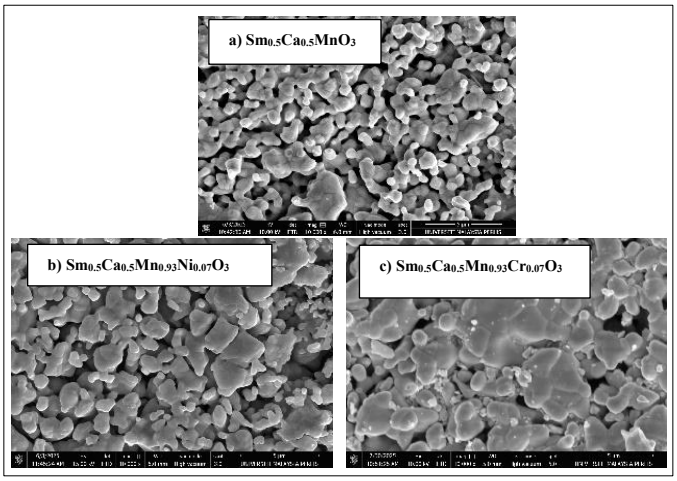

Fig. 2(a)-(c). FESEM micrographs (10000×) of divalent-doped $Sm_{0.5}Ca_{0.5}MnO_3$, $Sm_{0.5}Ca_{0.5}Mn_{0.93}Ni_{0.07}O_3$ and $Sm_{0.5}Ca_{0.5}Mn_{0.93}Cr_{0.07}O_3$ samples.

For the Ni-substituted sample $Sm_{0.5}Ca_{0.5}Mn_{0.93}Ni_{0.07}O_3$ the unit cell volume slightly increases to 209.607Å^3. This minor expansion suggests that Ni^{2+} ions are most likely substituting Mn^{3+} ions rather than Mn^{4+}, due to their comparable Ni^{2+} (0.69 Å) and Mn^{3+} (0.65 Å) ionic radii which are both significantly larger than that of Mn^{4+} (0.56 Å). A similar trend has been identified in other systems such as $Sm_{0.55}Sr_{0.45}Mn_{1-x}Ni_xO_3$ [11].

In contrast, the volume of the unit cell for the Cr-substituted sample, $Sm_{0.5}Ca_{0.5}Mn_{0.93}Cr_{0.07}O_3$, shows a slight decrease to 209.533 Å^3. This decrease is due to the smaller ionic radius of Cr^{3+} (0.615 Å) related to Mn^{3+} (0.65 Å), indicating that Cr^{3+} likely replaces Mn^{3+} in the lattice. Similar findings have been reported in previous studies involving Cr substitution, such as in $Pr_{0.75}Na_{0.05}K_{0.20}Mn_{1-x}Cr_xO_3$ [12].

Further, additional analysis was performed by calculating the tolerance factor (τ) [4,13] to assess and validate the stability of the crystal structure of the samples under study in Equation (1):

$$\tau = (< r_A > + < r_O > / \sqrt{2} < r_B > + < r_O) \quad (1)$$

where the average ionic radii of the A-site $< r_A >$ and B-site $< r_B >$, along with the ionic radius of oxygen $< r_O >$. The calculated tolerance factor (τ) for $Sm_{0.5}Ca_{0.5}MnO_3$ and $Sm_{0.5}Ca_{0.5}Mn_{0.93}Ni_{0.07}O_3$ and $Sm_{0.5}Ca_{0.5}Mn_{0.93}Cr_{0.07}O_3$ achieved samples varies which is 0.9094, 0.8949 and 0.9008 as presented in Table 1, signifying that all samples reside within the orthorhombic structural domain and demonstrate no substantial structural deformation. This discovery aligns with prior reports indicating that substances with τ values under 0.96 typically crystallise in the orthorhombic perovskite structure [5,14,15].
In addition to the above analysis, the variance in Jahn-Teller (JT) distortion, denoted as σ^2_{JT}., was also evaluated to quantify the degree of distortion in the MnO_6 octahedra. This parameter is expressed as follows [4]:

$$\sigma^2_{JT} = 1/6 \sum [d_{(Mn\text{-}O)i} - d_{< Mn\text{-}O >} / d_{< Mn\text{-}O >}]^2 \quad (2)$$

where, $d_{(Mn\text{-}O)}$ represents the individual Mn–O bond distances, while $d_{< Mn\text{-}O >}$ denotes the average Mn–O bond length. As shown in Table 1, the octahedral distortion decreased with increasing Ni^{2+} and Cr^{3+} content, as indicated by the declining calculated values of σ^2_{JT}.

The temperature-dependent resistivity of $Sm_{0.5}Ca_{0.5}MnO_3$, $Sm_{0.5}Ca_{0.5}Mn_{0.93}Ni_{0.07}O_3$ and $Sm_{0.5}Ca_{0.5}Mn_{0.93}Cr_{0.07}O_3$ samples was measured over the range 30-300 K in the presence of applied magnetic fields of 0 T and 0.8 T. The resistivity vs. temperature plots are shown in Fig. 3 (a)-(c) for all compositions under both field conditions. For the pure compound, in Fig. 3 (a) the resistivity stays consistently high across the entire temperature range, indicating characteristic insulating behaviour without any observable T_{MI}. This is due to Mn^{3+} ions in MnO_6 octahedra causing lattice distortions. The distortions entrap electrons, resulting in the formation of Jahn-Teller (JT) polarons. JT polarons block electron mobility, hence enhancing resistivity and reinforcing the insulating state. For Fig. 3 (b), upon introduce Ni^{2+} at x= 0.07 the samples still behave as insulators, but with noticeably reduced resistivity compared to x = 0. The decrease in resistivity below 60 K for the $Sm_{0.5}Ca_{0.5}Mn_{0.93}Ni_{0.07}O_3$ sample indicates that Ni^{2+} substitution facilitates the delocalisation of certain charge carriers. This occurs as Ni^{2+} substitutes for Mn^{3+}, which is a JT active ion. The absence of Mn^{3+} diminishes the Jahn-Teller distortion (σ^2_{JT}) and lessens electron-phonon interactions. Nonetheless, the ferromagnetic (FM) the association between Ni^{2+} and Mn^{4+} may be insufficient to entirely inhibit the antiferromagnetic charge-ordered (AFM-CO) state [16]. Consequently, antiferromagnetic interactions among Mn^{4+}-Mn^{4+} and Mn^{3+}-Mn^{3+} prevail, hence the material continues to exhibit insulating properties. Ni acts as an effective disorder agent because its Ni^{2+} state disrupts both the electronic continuity and magnetic exchange pathways within the Mn-O-Mn network, weakening double-exchange interactions essential for ferromagnetic coherence. The associated ionic size mismatch and e_g electron deficiency introduce local lattice distortions and competing superexchange interactions, which raise the energetic cost for ferromagnetic clusters to merge. However, the Ni^{2+} with 0.07 concentrations is insufficient to fully suppress the CO state or trigger a transition to metallic behaviour, consistent with previous reports [17]. In contrast, substitution of Cr^{3+}, which was $Sm_{0.5}Ca_{0.5}Mn_{0.93}Cr_{0.07}O_3$ (Fig. 3(c)) sample lead to notable changes in electrical behaviour. As seen in Fig. 3c) compositions exhibit clear MI transitions. The T_{MI} occurs at 55 K under zero field and shifts to 75 K with a 0.8 T field. These results demonstrate that Cr^{3+} substitution effectively suppresses the CO state and promotes a FMM phase. The observed T_{MI} at 55 K, accompanied by a significant drop in resistivity, is likely attributed to the development of FM interactions amid Mn^{3+}-O-Cr^{3+}, where the DE mechanism becomes dominant, effectively suppressing the CO state [12]. The introduction of Cr^{3+} which shares the corresponding electronic configuration as Mn^{4+} disrupts the CO within the Mn lattice. This disruption facilitates electron hopping across Mn^{3+}-Mn^{3+} pathways, promoting charge carrier delocalization and strengthening the DE interaction [12,18]. Other than that, the inducement occurs because Cr^{3+} reduces the strength of JT distortions, which is measured by (σ^2_{JT}). A higher (σ^2_{JT}) means stronger distortion and higher resistivity, while a lower (σ^2_{JT}) means weaker distortion and lower resistivity. Moreover, the substitution of Cr^{3+}, a magnetic ion, affects with the long-range

Table 1. Structure parameter, Average bond distance, d < Mn-O > and angle, <Mn-O-Mn>; Good fitness χ^2; Average ionic radius at A-site; $< r_A >$; Average ionic radius at B-site, $< r_B >$; Tolerance factor, τ; JT variance, σ^2_{JT}; $Sm_{0.5}Ca_{0.5}MnO_3$, $Sm_{0.5}Ca_{0.5}Mn_{0.93}Ni_{0.07}O_3$ and $Sm_{0.5}Ca_{0.5}Mn_{0.93}Cr_{0.07}O_3$.

Sample(x)	$Sm_{0.5}Ca_{0.5}MnO_3$	$Sm_{0.5}Ca_{0.5}Mn_{0.93}Ni_{0.07}O_3$	$Sm_{0.5}Ca_{0.5}Mn_{0.93}Cr_{0.07}O_3$
Lattice parameter			
***a* (Å)**	5.32890	5.32622	5.32351
***b* (Å)**	7.44629	7.44943	7.45408
***c* (Å)**	5.27962	5.28279	5.28032
Volume, *V* (Å^3)	209.498	209.607	209.533
Average			
Bond distance, d < Mn-O > (Å)	1.8261	1.8893	1.9227
Bond angle, <Mn-O-Mn> (°)	157.9	155.15	155.4
Good fitness, χ^2	1.956	2.220	1.435
Concentration Mn^{3+}	0.50	0.36	0.29
Concentration Mn^{4+}	0.50	0.64	0.71
Average ionic radius, $<r_A>$ (Å)	1.1560	1.1560	1.1560
Average ionic radius, $<r_B>$ (Å)	1.9875	2.0197	2.0064
Tolerance factor, τ	0.9094	0.8949	0.9008
JT Variance, σ^2_{JT} ($x10^{-3}$ Å^2)	0.6940	0.0240	0.0492

antiferromagnetic (AFM) order which particularly the Mn^{3+}-Mn^{3+} and Mn^{4+}-Mn^{4+} super exchange interactions, thereby breaking AFM spin alignment [12,19]. This leads to the emergence of FM relations, especially connecting Mn^{3+} and Mn^{4+} ions.

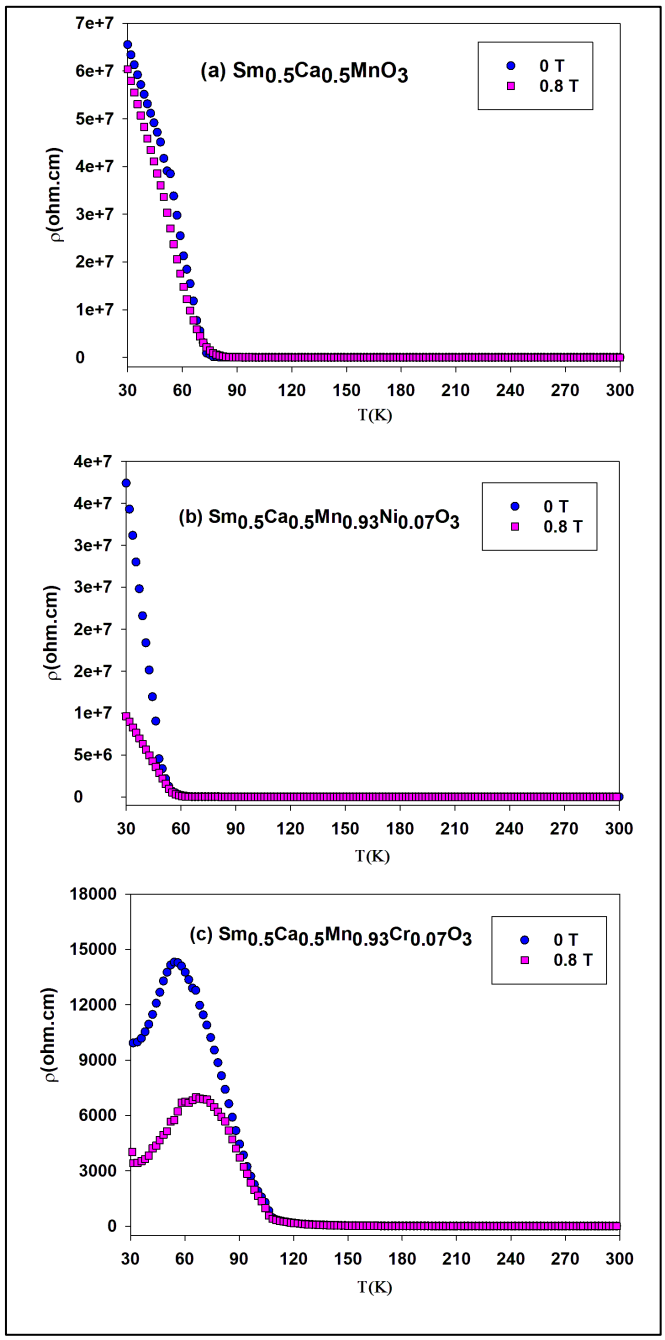

Fig. 3(a)-(c). Resistivity vs temperature curves for $Sm_{0.5}Ca_{0.5}MnO_3$, $Sm_{0.5}Ca_{0.5}Mn_{0.93}Ni_{0.07}O_3$ and $Sm_{0.5}Ca_{0.5}Mn_{0.93}Cr_{0.07}O_3$ below magnetic field of 0 and 0.8 T.

Next, the magnetoresistance percentage (MR %) with respect to temperature under an applied external field of 0.8 T for all samples is illustrated in the Fig. 4. The MR percentage was computed with Equation (3) which is expressed as follows [5, 14, 20].

$$MR(\%)\frac{\rho(0,T)-\rho(H,T)}{\rho(0,T)}\times 100\% \quad (3)$$

where $\rho\ (0,T)$ denotes the resistivity without a magnetic field, and $\rho\ (H,T)$ represents the resistivity underneath an external magnetic field.

The MR behavior of $Sm_{0.5}Ca_{0.5}MnO_3$, $Sm_{0.5}Ca_{0.5}Mn_{0.93}Ni_{0.07}O_3$ and $Sm_{0.5}Ca_{0.5}Mn_{0.93}Cr_{0.07}O_3$ was investigated under an external magnetic field of 0.8 T. The MR behavior of $Sm_{0.5}Ca_{0.5}MnO_3$ was very low and small value which is 8.89% until temperature reached to 60K and decreased. The sample resistivity continued unchanged under magnetic field, 0.8T. It is due that strong charge carrier localisation and the emergence of a CO–AFM state phase. Concerning the sample with Ni^{2+} substitution $Sm_{0.5}Ca_{0.5}Mn_{0.93}Ni_{0.07}O_3$, the MR starts to about 30 K and reaches a value of about 55.25%. This behaviour suggests that an extrinsic MR effect has appeared, which is probably due to spin-polarized tunnelling across grain boundaries [5,21]. When the application of an external magnetic field, and alignment of the spins associated with charge carriers thus inhibiting the CO-AFM phase. This suggested that an increased number of spin-polarized electrons can cross the grain boundaries, hence enhancing the material's total magnetoresistance response at low temperatures [4,5]. This trend is further supported by the FESEM results in Fig. 2(b), where substitution Ni^{2+} concentration results in grain size growth accompanied by a reduction in grain boundary density. For the sample with Cr^{3+} substitution $Sm_{0.5}Ca_{0.5}Mn_{0.93}Cr_{0.07}O_3$, the MR starts to rise slowly around 30 K, reaches its peak MR point of about 62.86% at about 46 K, and then slowly falls at lower temperatures. The clear MR peak near the T_{MI} in these sample unlike the undoped and Ni^{2+} substitution. The intrinsic MR effect that is usually linked to strong dominant intrinsic MR, originating from the DE mechanism [4,22]. The impact of grain boundaries on MR is demonstrated in FESEM analysis in Fig. 2(c). The reduction in grain boundary resulting from Cr^{3+} substitution suggests improved grain connectivity. This is suggested that Cr^{3+} substitution assistances suppress spin fluctuations and enhance spin alignment under magnetic field.

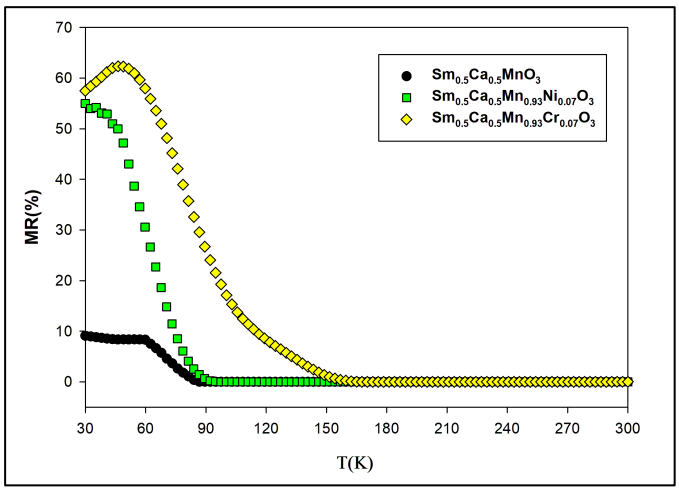

Fig. 4. Magnetoresistance percentage, MR (%), vs temperature for $Sm_{0.5}Ca_{0.5}MnO_3$, $Sm_{0.5}Ca_{0.5}Mn_{0.93}Ni_{0.07}O_3$ and $Sm_{0.5}Ca_{0.5}Mn_{0.93}Cr_{0.07}O_3$

4. CONCLUSION

In summary, this study demonstrates that partial substitution of Mn-site ions in $Sm_{0.5}Ca_{0.5}MnO_3$ with Ni^{2+} and Cr^{3+} at x= 0.07 significantly alters its structural and electrical transport properties, offering insights into mechanisms for destabilizing the CO state. Both dopants maintain the orthorhombic *Pnma* structure, but their effects diverge due to differences in ionic size and electronic configuration. Ni^{2+} substitution slightly increases unit cell volume and reduces resistivity without inducing a metallic phase, suggesting limited suppression of CO. In contrast, Cr^{3+} substitution more effectively reduces Jahn-Teller distortion and induces a T_{MI}, clearly signalling CO suppression and enhancement of DE driven FMM behaviour. These results highlight Cr^{3+} as a more effective dopant than Ni^{2+} for promoting metallicity in charge-ordered manganites, making it a promising candidate for modifying materials for magnetoresistive and spintronic applications. Cr^{3+} substitution in $Sm_{0.5}Ca_{0.5}MnO_3$ creates the strongest MR response by enhancing spin alignment and suppressing spin fluctuations, unlike the weak MR in the pure compound and the extrinsic MR in the Ni^{2+} substituted sample The present findings provide a foundation for the systematic investigation of additional B-site substitution with different valence states and ionic radii to further optimize the interplay among charge ordering, double exchange, and lattice distortions in half-doped manganites. Future studies focusing on different of substitution concentration effects, detailed magnetic phase diagrams, and advanced microscopic techniques such as neutron diffraction and X-ray absorption spectroscopy could offer deeper insight into the coupled structural, magnetic, and electronic interactions.

ACKNOWLEDGEMENT

The authors would like to acknowledge the support of Universiti Teknologi Mara (UiTM) Perlis Branch and Faculty of Applied Sciences, UiTM Shah Alam for providing the facilities for this research. This research was supported by the Ministry of Higher Education through the Fundamental Research Grant Scheme (Grant No.: FRGS/1/2023/STG07/UITM/02/9).

REFERENCES

[1] Wang, H., Zhang, H., Su, K., Huang, S., Tan, W., & Huo, D. (2020). Structure, charge ordering, and magnetic properties of perovskite $Sm_{0.5}Ca_{0.5}MnO_3$ manganite. Journal of Materials Science: Materials in Electronics, 31(17), 14421–14425. doi: https://doi.org/10.1007/s10854-020-04001-6

[2] Giri, S. K., Yusuf, S. M., Mukadam, M. D., & Nath, T. K. (2014). Enhanced exchange bias effect in size modulated $Sm_{0.5}Ca_{0.5}MnO_3$ phase separated manganite. Journal of Applied Physics, 115(9). doi: https://doi.org/10.1063/1.4867523

[3] Xu, X., Li, Y., Hou, F., Cheng, Q., & Su, R. (2015). Effect of Co substitution on magnetic ground state in $Sm_{0.5}Ca_{0.5}MnO_3$. Journal of Alloys and Compounds, 628, 89–96. doi: https://doi.org/10.1016/j.jallcom.2014.12.116

[4] Rozilah, R., Ibrahim, N., & Yahya, A. K. (2019). Inducement of ferromagnetic–metallic phase and magnetoresistance behavior in charged ordered monovalent-doped $Pr_{0.75}Na_{0.25}MnO_3$ manganite by Ni substitution. Solid State Sciences, 87, 64–80. doi: https://doi.org/10.1016/j.solidstatesciences.2018.11.005

[5] Ariffiin, M., Ibrahim, N., Mohamed, Z., Yahya, A. K., Khan, N. A., & Khan, M. N. (2018). Revival of Metal-Insulator and Ferromagnetic-Paramagnetic Transitions by Ni Substitution at Mn Site in Charge-Ordered Monovalent Doped $Nd_{0.75}Na_{0.25}MnO_3$ Manganites. Journal of Superconductivity and Novel Magnetism, 31(9), 2851–2868. doi: https://doi.org/10.1007/s10948-017-4521-7

[6] Das, K., Banu, N., Das, I., & Dev, B. N. (2018). Magnetocaloric effect of polycrystalline $Sm_{0.5}Ca_{0.5}MnO_3$ compound: Investigation of low temperature magnetic state. Solid State Communications, 274, 36–40. doi: https://doi.org/10.1016/j.ssc.2018.02.014

[7] Li, Y., Cheng, Q., & Qi, D. (2012). CERAMICS Effects of Al doping upon ac susceptibility of $Pr_{0.5}Ca_{0.5}MnO_3$. doi: https://doi.org/10.1016/j.ceramint.2012.07.072

[8] Liu, Y., Kong, H., & Zhu, C. (2007). Coexistence of charge ordering and ferromagnetism in $Nd_{0.5}Ca_{0.5}Mn_{1-x}Co_xO_3$ ($x \leq 0.1$). Journal of Alloys and Compounds, 439(1–2), 33–36. doi: https://doi.org/10.1016/j.jallcom.2006.08.315

[9] Pi, L., Hébert, S., Yaicle, C., Martin, C., Maignan, A., & Raveau, B. (2003). The $Pr_{0.5}Ca_{0.5}Mn_{1-x}Cr_x O_3$ series (0 x 0.5): evidence of steps in the magnetic and transport properties for a narrow composition range. In J. Phys.: Condens. Matter (Vol. 15). doi: https://doi.org/10.1088/0953-8984/15/17/322

[10] Rajmi, R. (2023). Revival of Ferromagnetic-Metallic Phase and Emergence of Griffiths Phase via Ni and Cr Substitution in Charged-Ordered $Pr_{0.75}Na_{0.25}MnO_3$ Manganite. Scientific Research Journal, 20(2), 53–69. doi: https://doi.org/10.24191/srj.v20i2.22185

[11] Abdelhadi, M. M., & Ziq, K. A. (2013). Effect of mn-site doping with nickel on the electric and magnetic properties of $Sm_{0.55}Sr_{0.45}MnO_3$ manganites. Journal of Superconductivity and Novel Magnetism, 26(5), 1445–1450. doi: https://doi.org/10.1007/s10948-012-1945-y

[12] Sumaiyah, S., Ibrahim, N., Mohamed, Z., Rozilah, R., Kazmi, J., Masood, A., & Muhammed Ali, S. (n.d.). Tuning magnetic interaction by Cr substitution in Pr-based $Pr_{0.75}Na_{0.05}K_{0.20}Mn_{1-x}Cr_xO_3$ (x = 0-0.05) monovalent doped manganites. doi: https://doi.org/10.2139/ssrn.4536478

[13] Bartel, C. J., Sutton, C., Goldsmith, B. R., Ouyang, R., Musgrave, C. B., Ghiringhelli, L. M., & Scheffler, M. (2019). New tolerance factor to predict the stability of perovskite oxides and halides. doi: https://doi.org/10.1126/sciadv.aav0693

[14] Rozilah, R., Ibrahim, N., Mohamed, Z., Yahya, A. K., Khan, N. A., & Khan, M. N. (2017). Inducement of ferromagnetic-metallic phase in intermediate-doped charge-ordered $Pr_{0.75}Na_{0.25}MnO_3$ manganite by K+ substitution. Physica B: Condensed Matter, 521, 281–294. doi: https://doi.org/10.1016/j.physb.2017.07.001

[15] Smari, M., Hamouda, R., Walha, I., Dhahri, E., Mompeán, F. J., & García-Hernández, M. (2015). Magnetic and magnetoresistance in half-doped manganite $La_{0.5}Ca_{0.5}MnO_3$ and $La_{0.5}Ca_{0.4}Ag_{0.1}MnO_3$. Journal of Alloys and Compounds, 644, 632–637. doi: https://doi.org/10.1016/j.jallcom.2015.05.026

[16] Bhaskar, A., Huang, M. S., & Liu, C. J. (2018). Suppression of charge ordering and thermal hysteresis of electronic transport and magnetisation in $La_{0.5}Ca_{0.5}Mn_{1-x}Ni_xO_3$. Philosophical Magazine, 98(2), 139–154. doi: https://doi.org/10.1080/14786435.2017.1396376

[17] Oumezzine, M., Peña, O., Kallel, S., Guizouarn, T., & Oumezzine, M. (2012). Structural studies and magnetic and transport properties of Cr-substituted $La_{0.67}Ba_{0.33}Mn_{1-x}Cr_xO_3$ ($0 \leq x \leq 0.15$) perovskites. Journal of Alloys and Compounds, 533, 33–40 doi: https://doi.org/10.1016/j.jallcom.2012.04.026

[18] Carneiro, A. S., Fonseca, F. C., Jardim, R. F., & Kimura, T. (2003). Phase coexistence in Cr-doped $Nd_{0.5}Ca_{0.5}MnO_3$ compounds. Journal of Applied Physics, 93(103), 8074–8076. doi: https://doi.org/10.1063/1.1540181

[19] Asmira, N., Ibrahim, N., Mohamed, Z., & Yahya, A. K. (2018). Effect of Cr^{3+} substitution at Mn-site on electrical and magnetic properties of charge ordered $Bi_{0.3}Pr_{0.3}Ca_{0.4}MnO3$ manganites. Physica B: Condensed Matter, 544, 34–46. doi: https://doi.org/10.1016/j.physb.2018.05.020

[20] Vitayaya, O., Zul Nehan, P. Z., Munazat, D. R., Manawan, M. T. E., & Kurniawan, B. (2024). Magnetoresistance (MR) properties of magnetic materials. In RSC Advances (14(26), 18617–18645). doi: https://doi.org/10.1039/d4ra01989j

[21] Zahrin, A., Azhar, N. A., Ibrahim, N., & Mohamed, Z. (2022). Structural, Magnetic, and Electrical Properties and Magnetoresistance of Monovalent K-Substituted $La_{0.7}Ba_{0.3-x}K_xMnO_3$ (x=0 and 0.04) Manganite. Condensed Matter, 7(3). doi: https://doi.org/10.3390/condmat7030051

[22] Zawawi, R. A., Ibrahim, N., & Shamsuddin, S. (2018). Enhancement of Double-Exchange Mechanism in Charge-Ordered $Pr_{0.7}Na_{0.25}MnO_3$ Ceramics by Cr Doped at Mn-Site. International Journal of Current Research in Science, Engineering & Technology, 1(Spl-1), 101. doi: https://doi.org/10.30967/ijcrset.1.s1.2018.101-105